processes

MDPI

Article

Highly Efficient and Rapid Removal of Methylene Blue from Aqueous Solution Using Folic Acid-Conjugated Dendritic Mesoporous Silica Nanoparticles

Abdurrahman A. Almethen [1,†], Khalid Mohammed Alotaibi [2,*,†], Haitham S. Alhumud [1] and Abdullah M. Alswieleh [2,*,†]

[1] King Abdulaziz City for Science and Technology, Riyadh 11442, Saudi Arabia; amethen@kacst.edu.sa (A.A.A.); halhamoud@kacst.edu.sa (H.S.A.)
[2] Department of Chemistry, College of Science, King Saud University, Riyadh 11451, Saudi Arabia
* Correspondence: khalid.m@ksu.edu.sa (K.M.A.); aswieleh@ksu.edu.sa (A.M.A.)
† These authors contributed equally to this work.

Abstract: Dendritic Mesoporous Silica Nanoparticles (DMSNs) are considered superior in the adsorption of unfavorable chemical compounds and biological pollutants. Herein, we have synthesized folic acid-terminated dendritic mesoporous silica nanoparticles (FA-DMSN) for the removal of cationic dyes, methylene blue (MB), from aqueous solutions. The structural, morphological, functional, specific surface area, pore size distribution, and thermal properties of the synthesized DMSNs were identified using a scanning electron microscope (SEM), a transmission electron microscope (TEM), Fourier transform infrared spectroscopy (FTIR), dynamic light scattering (DLS), Brunauer−Emmett−Teller (BET), and Thermogravimetric Analyzer (TGA). The synthesized DMSNs exhibited a high surface area (521 $m^{2\ -1}$) and pore volume (1.2 $cm^3\ g^{-1}$). In addition, it features both wide pore size and narrow distributions, which strongly affect the adsorption performance in terms of the equilibrium uptake time. Moreover, the impact of pH, contacting time, and dye's initial concentration on the removal efficiency of MB was studied. The extraction efficiency of FA-DMSN was found to be three times more effective than the bare DMSN materials. Langmuir isotherm fitted the experimental data very well with a correlation coefficient value of 0.99. According to the Langmuir model, the maximum adsorption capacity was 90.7 mg/g. Furthermore, the intra−particle diffusion model revealed a significantly fast intra-particle diffusion which can be attributed to the presence of the large pore's channels. Finally, the fast adsorption of MB molecules, reaching their equilibrium capacity within tens of seconds, as well as the low cost and ease of FA-DMSN fabrication, makes the developed material an effective adsorbent for water remediations.

Keywords: dendritic mesoporous silica nanoparticles; amine-functionalization; folic acid-conjugation; cationic dyes; dyes removal

Citation: Almethen, A.A.; Alotaibi, K.M.; Alhumud, H.S.; Alswieleh, A.M. Highly Efficient and Rapid Removal of Methylene Blue from Aqueous Solution Using Folic Acid-Conjugated Dendritic Mesoporous Silica Nanoparticles. *Processes* **2022**, *10*, 705. https://doi.org/10.3390/pr10040705

Academic Editor: María Victoria López Ramón

Received: 17 March 2022
Accepted: 2 April 2022
Published: 5 April 2022

1. Introduction

Growing water scarcity is one of the biggest threats to societies and the world nowadays. As long as there is a continuous growth in the global population, industrial development, and climate change, water scarcity will exacerbate in the future. Currently, the wide use of dyes in various applications, such as textile dyes, biological dyes, printing inks, and drugs, resulted in the discharge of untreated effluents into freshwater systems [1]. These dyes affect the water purity and hinder the light from penetrating through water [2]. Consequently, decreasing the level of dissolved oxygen and the rate of photosynthesis can harm the entire aquatic biota [2,3]. Thus, there is an urgent need to develop treatment strategies to ensure a healthy and sustainable environment for the future generation.

Several physical, chemical, and biological water remediation techniques have been used, such as adsorption, filtration, coagulation/flocculation, ion-exchange, advanced

oxidation processes, activated sludge processes, and membrane bioreactors [4–8]. Among these techniques, adsorption is considered to be the most widely utilized for the removal of potentially toxic elements and organic pollutants from wastewater [9,10].

The use of mesoporous materials as an adsorbent, in particular, mesoporous silica nanoparticles (MSNs) has gained great interest due to their high specific surface area, uniform and tunable pore diameter, and the easy modification of their structure and physical properties. In the last three decades, various types of MSNs materials, for instance, SBA-15, SBA-16, MSM-41, and MCM-48, bioinspired silica, and silica aerogels have been reported with a wide variety of shapes and sizes [11–14].

A new family of MSNs was initially reported, known as dendritic fibrous silica-based nanoparticles (DMSNs) that has large radial pore structures and high accessible surface [15]. As a unique category of MSNs, dendritic mesoporous silica nanoparticles could be modified with various organic functional groups to enhance their physical and chemical properties further. Moreover, the excellent pore accessibility of DMSNs could prevent the possibility of the channel's blockage even in the presence of a high concentration of functional groups. DMSNs show a specific surface area ranging from 450 to 900 $m^2 \cdot g^{-1}$ that can be controlled by manipulating the density and pore size of the fibers [16]. Unlike conventional silica nanomaterials, DMSNs have a wide pore size distribution, with the channel being divergently grown from the center of the nanoparticles.

Interestingly, DMSNs possess high thermal, chemical, and mechanical stability, which can be used in different applications, especially when durability is required. Another characteristic property of DMSNs is their nontoxicity and biocompatibility, making them an excellent candidate for many biomedical applications [17–19].

Maryam et al. [20] reported the synthesis of d-penicillamine-modified DMSNs for the removal of Pb^{2+}, Ni^{2+}, Co^{2+}, and Ag^{+} ions from aqueous media. The results show that selective adsorption of the targeted ions can be achieved. Nia et al. [21] designed DMSNs that were internally cross-linked using bivalent 1,4-diazabicyclo[2.2.2]octane to be used as an adsorbent for dyes mixture. The material exhibits efficient binding sites for methylene blue ions and for Procion Red MX-5B. Abbasvash et al. [22] reported the preparation of β-cyclodextrin modified DMSNs for the removal of malachite green dye. More than 92% removal efficiency was achieved using the proposed materials.

The functionalization of mesoporous silica nanoparticles with folic acid has been widely used as a targeting ligand for cancer cells that have folic acids receptors which are located in several cancers, such as brain, lung and breast cancers [23]. Abouaitah et al. [24] reported the synthesis of two types of MSNs: MCM-41 and KCC-1 that were functionalized using the folic acid functional group and used as vehicles to transport the natural prodrugs COL, CR, and QR into hepatocellular carcinoma cells (HepG2). The results show that KCC-1 type MSNs exhibited higher intracellular uptake than MCM-41. Wei et al. [25] studied the preparation of folic acid-conjugated MSNs to improve the therapeutic efficacy of topotecan to treat retinoblastoma (RB) cancers. The results clearly show that folic acid-conjugated MSNs significantly enhanced cellular uptake compared to non-targeted nanoparticles. To the best of our knowledge, no studies have investigated the modification of DMSNs with the folic acid functional group as an adsorbent for the removal of cationic dyes from aqueous solutions

In this study, easily accessible dendritic pores channels mesoporous silica nanoparticles were synthesized and modified with the folic acid functional group. DMSNs with center-radial oriented large and open mesopores can easily provide accessible space for faster molecular diffusion. Therefore, cationic dye, such as methylene blue has been chosen as a model molecule to investigate the uptake characteristics of the FA-DMSNs materials. The effect of pH, contacting time, and dye's initial concentration on the removal efficiency of MB was thoroughly studied. In order to understand the adsorption mechanisms of MB into the material's surface as well as their kinetic, several models were applied to the obtained experimental data, such as Langmuir and Freundlich isotherms, pseudo-first-order, pseudo-second-order, and intraparticle models.

2. Materials and Methods

2.1. Materials and Instruments

Material

Cetrimonium bromide (CTAB, 98%, Thermo Fisher Scientific, Waltham, MA, USA), Urea ($CO[NH_2]_2$, 99.0%, Fluka Chemie AG, Bux, Switzerland), Cyclohexane (ACS grade, 99.0%, Sigma-Aldrich, St. Louis, MO, USA), 2-propanol (HPLC grade, 99.9%, Sigma-Aldrich, USA), Ethanol (HPLC grade, 99.8%, Sigma-Aldrich, USA), tetraethylorthosilicate (TEOS, 98%, Thermo Fisher Scientific, USA), Acetone (ACS grade, 99.5%, Sigma-Aldrich, USA), Acetic acid (CH_3COOH, 99%, Interchem, Gillingham, UK), and Hydrogen peroxide (H_2O_2, 33% w/v [110 vol.], pharma grade, AppliChem GmbH, Darmstadt, Germany). Toluene (ACS grade, 99.5%, Sigma-Aldrich, USA) and (3-Aminopropyl)triethoxysilane (APTES, ≥98%, Sigma-Aldrich, USA). Folic Acid (FA, ≥97%, Sigma-Aldrich, USA), Dimethyl sulfoxide (DMSO, CAS No. 67-68-5, 99.8%, Loba Chemie Pvt. Ltd., Maharashtra, India) N,N′-dicyclohexylcarbodiimide (DCC, 99%. Sigma-Aldrich, USA), Triethylamine (TEA, CAS No. 121-44-8, 99.5%, Loba Chemie Pvt. Ltd. India), and N-Hydroxysuccinimide (NHS, ≥99.0%, Sigma-Aldrich, USA). All syntheses were performed using Elga purelab water system (15 MΩ cm, 25 °C).

2.2. Methods

2.2.1. Preparation of Dendritic Mesoporous Silica Nanoparticles (DMSNs)

1.0 g of CTAB was dissolved in 30 mL of DI water. Then, 0.6 g of urea was added with stirring for 5 min. Thereafter, a solution of 30 mL cyclohexane and 1.17 mL isopropyl alcohol was added to the mixture and further stirred for 2 h at room temperature; 2.7 mL of tetraethyl orthosilicate (TEOS) was added dropwise to the mixture. After the complete addition of TEOS, the reaction temperature was kept at 90 °C for 20 h [26]. Finally, the resulting nanoparticles were centrifuged and washed with ethanol and DI water several times.

The removal of the surfactant was achieved using a mixture of acetic acid and hydrogen peroxide with a volume ratio of 1:1. Typically, 30 mL of acetic acid was added to 30 mL of hydrogen peroxide at 120 °C with mild stirring for 24 h. The solid sample of DMSNs was collected using centrifugation and washed thoroughly with ethanol and water. The collected sample was dried in the oven for 24 h at 60 °C.

2.2.2. Amine-Surface Functionalization of DMSNs (AP-DMSN)

Two grams of DMSNs was dispersed in 50 mL of Toluene. Then 0.5 mL of APTES was added, and the mixture was refluxed for 24 h under stirring at 120 °C. The solid sample of DMSNs was collected using centrifugation and washed thoroughly with ethanol and water. The collected sample was dried in the oven for 24 h at 60 °C.

2.2.3. Folic Acid (FA-) Conjugated DMSNs (FA-DMSN)

An amount of 2.50 g of Folic Acid (FA) was dissolved in 50 mL of Dimethylsulfoxide (DMSO) and stirred for 15 min. Triethylamine (1.30 mL), NHS (1.30 g), and DCC (2.30 g) were added to the mixture. The mixture was stirred overnight at room temperature and kept in a dark environment. Next, the by-product was eliminated by filtration using glass fiber paper; 0.50 g of AP-DMSNs was added to 25 mL of the aliquot and stirred at 25 °C overnight [27,28]. The solid sample of DMSNs-FA was collected using centrifugation and washed thoroughly using DMSO and ethanol. The collected sample was then dried in the oven for 24 h at 60 °C.

2.3. Material Characterization

Scanning electron microscopy (SEM) and Transmission electron microscopy (TEM) images were performed via JSM-7100F thermal field scanning electron microscope at 15.0 kV and JEM-1400Flash Electron Microscope at 100 kV (JEOL Ltd., Tokyo, Japan), respectively, to study DMSNs' morphology. Fourier-transform infrared spectroscopy (FTIR) was conducted using spectrum BX FT-IR spectrometer (PerkinElmer Inc., Waltham, MA,

USA) with a wavenumber resolution of 2 cm^{-1} and the scanning range was between 4000 and 400 cm^{-1}. Dynamic light scattering (DLS) measurements were employed on Zetasizer Nano ZS (Malvern Panalytical, Morvin, UK) to determine the surface charges and the nanoparticles' sizes. UV measurements were obtained using Ultrospec Plus 4054 UV/Visible Spectrophotometer (LKB Biochrom Ltd., Cambridge, UK). Brunauer–Emmett–Teller (BET) surface area and pore size distribution of the DMSNs was carried out using Micromeritics Gemini 2375 volumetric analyzer (Micromeritics, Norcross, GA, USA).

2.4. Adsorption Experiments

The adsorption studies were performed via a thermostatic shaker at a shaking speed rate of 150 rpm. A stock solution of methylene blue (1000 $mg{\cdot}L^{-1}$) has been prepared by dissolving MB's analytical grade in deionized water. The pH of the studied solutions was adjusted using dilute solutions of hydrochloric acid and ammonium hydroxide. A fixed amount of the examined sorbents of 10 mg were added to a series of 15 mL centrifuge tubes containing a solution of MB and shaken at a speed rate of 150 rpm at room temperature. Different experimental variables were examined, including analyte concentration (50–125 $mg{\cdot}L^{-1}$), contact time (5–120 min), and pH (3–9) that can influence the adsorption efficiency of the materials. After the predetermined period of shaking time was conducted, the solutions were centrifuged at 7000 rpm, and the concentration of MB filtrate was analyzed using a UV/Visible spectrophotometer at a wavelength of 668 nm.

2.4.1. Adsorption Kinetics

The methylene blue (MB) adsorption kinetics data were analyzed by applying two adsorption kinetics models, namely the pseudo-first-order kinetic model and pseudo-second-order kinetic model [29–32].

Pseudo-First-Order Reaction Kinetic Model

The linear form of the pseudo-first-order reaction kinetic model can be represented as: [33,34]

$$log(Q_e - Q_t) = log(Q_e) - \frac{tK_1}{2.303} \quad (1)$$

where Q_t is the amount of adsorbate uptake from the aqueous solution per unit mass of adsorbent at time t (mgg^{-1}); K_1 is the adsorption rate constant of the pseudo-first-order kinetic ($L{\cdot}min^{-1}$).

Pseudo-Second-Order Reaction Kinetic Model

The pseudo-first-order reaction kinetic model is linearly given as the following expression: [35,36]

$$\frac{t}{Q_t} = \frac{1}{K_2 Q_e{}^2} + \frac{t}{Q_e} \quad (2)$$

where K_2 is the adsorption rate constant of the pseudo-second-order kinetic ($g{\cdot}mg^{-1}{\cdot}min^{-1}$)

The Intraparticle Diffusion Model

The particle diffusion mechanism was studied using Morris–Weber equation which is presented as follows: [37]

$$q_t = k_{id}\sqrt{t} \quad (3)$$

where q_t is the concentration of MB (mgl^{-1}) adsorbed at time t. k_{id} is the intraparticle diffusion rate constant.

2.4.2. Adsorption Isotherms

The equilibrium sorption isotherms of the targeted dye (MB) were studied with regard to Langmuir and Freundlich adsorption isotherms models. The mathematical Langmuir

and Freundlich adsorption isotherms nonlinear equations might be represented as shown below [30,38].

Langmuir Adsorption Isotherm Model

$$Q_e = \frac{K_L C_e}{1 + K_L C_e} Q_m \quad (4)$$

where Q_m is the maximum amount of dye adsorbed from the aqueous solution per unit mass of adsorbent (mg·g^{-1}); K_L is the Langmuir adsorption isotherm constant (L·mg^{-1}).

Freundlich Adsorption Isotherm Model

$$Q_e = K_F C_e{}^{\frac{1}{n}} \quad (5)$$

where K_F is the Freundlich adsorption isotherm constant (mg$^{1-\frac{1}{n}}$·L$^{\frac{1}{n}}$·g^{-1}); n is the adsorption intensity.

3. Results

3.1. Properties of Synthesized and Surface-Modified DMSNs

Figure 1 demonstrates scanning and transmission electron microscopy images of DMSN with and without the presence of the surfactant. As shown in Figure 1A–F, all the prepared nanoparticles exhibit a regular spherical shape containing center-radial pore channels. Moreover, no apparent effect of the surfactant removal method on the structure of the materials, Figure 1D–F. The average particle-size distribution of DMSN obtained using dynamic light scattering, Figure 2, was ca-340 nm which agreed well with the SEM and TEM results.

The surface characteristics of made-DAMSN, DAMSN, AP-DAMSN, and FA-DAMSN were preliminarily investigated by Brunauer–Emmett–Teller (BET). As shown in Figure 3, all the aforementioned materials exhibited obvious N_2 physisorption isotherms (IV-type), indicating the mesoporous nature of the materials [39]. The hysteresis loops (H1-type) P/P_0 for the DMSN appeared in the range of 0.4–0.7, indicating the presence of bimodal mesopores [40]. The specific surface area and the total pore volume of made−DMSN, DMSNs, AP-DMSN, and FA-DMSN were calculated and demonstrated in Table 1. The change in both BET surface area and total pore volume after each modification step implies the success of the proposed modification methods. The pore size distribution increases after the removal of the surfactant and reveals the bimodal mesopores with an average value of 25 and 120 A° Figure 3II. Moreover, a gradual reduction in the pore size distribution after each modification step results in a sharp change in the specific surface area and pore volume.

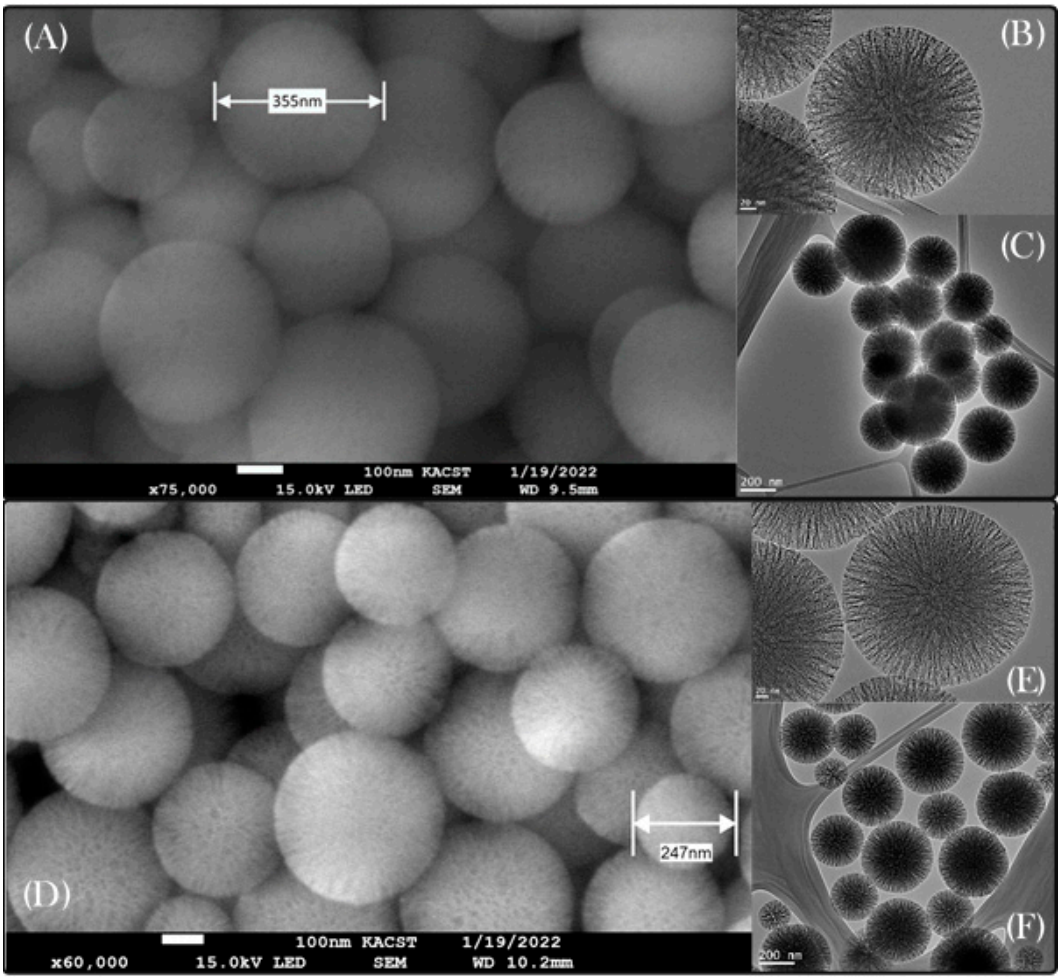

Figure 1. Electron microscopic images of the synthesized nanoparticles: (**A**) SEM image of as made−DMSN; (**B**,**C**) TEM images of as made−DMSN; (**D**) SEM image of DMSNs; (**E**,**F**) TEM images of DMSNs.

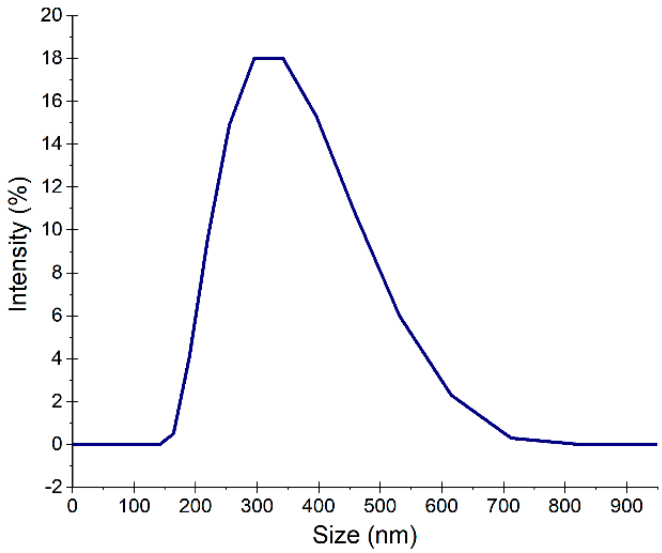

Figure 2. Particle size distribution of DMSNs.

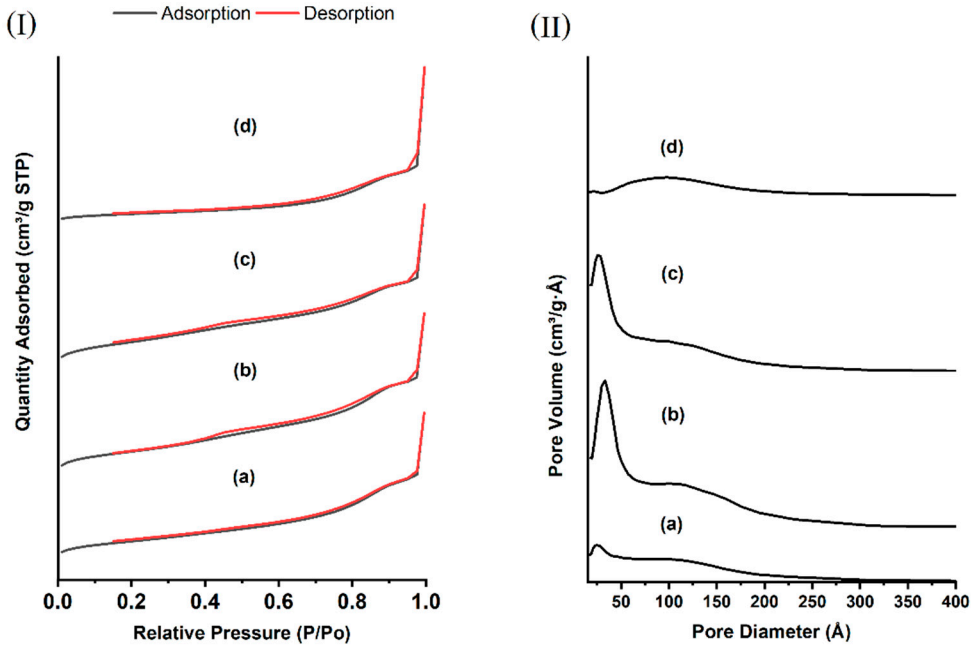

Figure 3. N_2 adsorption-desorption isotherm (BET) (**I**) and pore size distribution (**II**) for (**a**) as made−DMSN, (**b**) DMSNs, (**c**) AP-DMSN, and (**d**) FA-DMSN.

Table 1. Surface area and pore volume of DMSNs samples.

Sample	BET Surface Area ($m^2 \cdot g^{-1}$)	Pore Volume ($cm^3 \cdot g^{-1}$)
As made−DMSN	160.16	0.55
DMSN	520.93	1.21
AP-DMSN	382.54	0.97
FA-DMSN	53.14	0.56

The FT-IR spectra of the as-made DMSN, AP-DMSN, and FA-DMSN are shown in Figure 4. For as made DMSN (Figure 4a) several broad absorption bands assigned to Si−O−Si (1250–1030 cm^{-1}), Si−OH (804 cm^{-1}), −OH (3000–3450 cm^{-1}) and Si−O (465 cm^{-1}) [29,41,42]. The strong band at 2950 cm^{-1} and 2850 cm^{-1} correspond to the asymmetric and symmetric stretching vibration of the methylene groups of the carbon chain. The successful extraction of surfactant was confirmed by the disappearance of the characteristic bands at 2850–2950 cm^{-1}, Figure 4b. An increase in the peak intensity of the −OH group in the FA-DMSN compared to AP-DMSN was observed, confirming the grafting of folic acid moiety into the material's surface, Figure 4c, d. Moreover, the peak at 1450 cm^{-1} is assigned to an asymmetric stretching mode of the carboxylic acid group. Peaks at 1540, 1614 and 1650 cm^{-1} are attributed to C−N, C−C (in the aromatic ring), and N−H primary amine bending vibrations, respectively. Finally, the band at 1700 cm^{-1} corresponds to the carbonyl stretching vibration of the acidic and amide groups [43,44].

The average surface charge of both AP -DMSN and FA-DMSN was determined using Zeta potential analysis, Figure 5. It is well known that bare silica nanoparticles have an isoelectric point (IEP) of ca-2 with a surface being negatively charged at a pH higher than 2 [8]. After modifying the DMSNs with amino groups, the nanoparticle was changed to a highly positively charged surface at pH values ranging from 3 to 9 with an IEP value of around 10, Figure 5 (upper panel). Further modifying the surface with folic acid has resulted in shifting the surface charge from being highly positive to highly negative at all studied pH values Figure 5 (lower panel). The obtained results revealed that surface modification of DMSNs nanoparticles had been achieved.

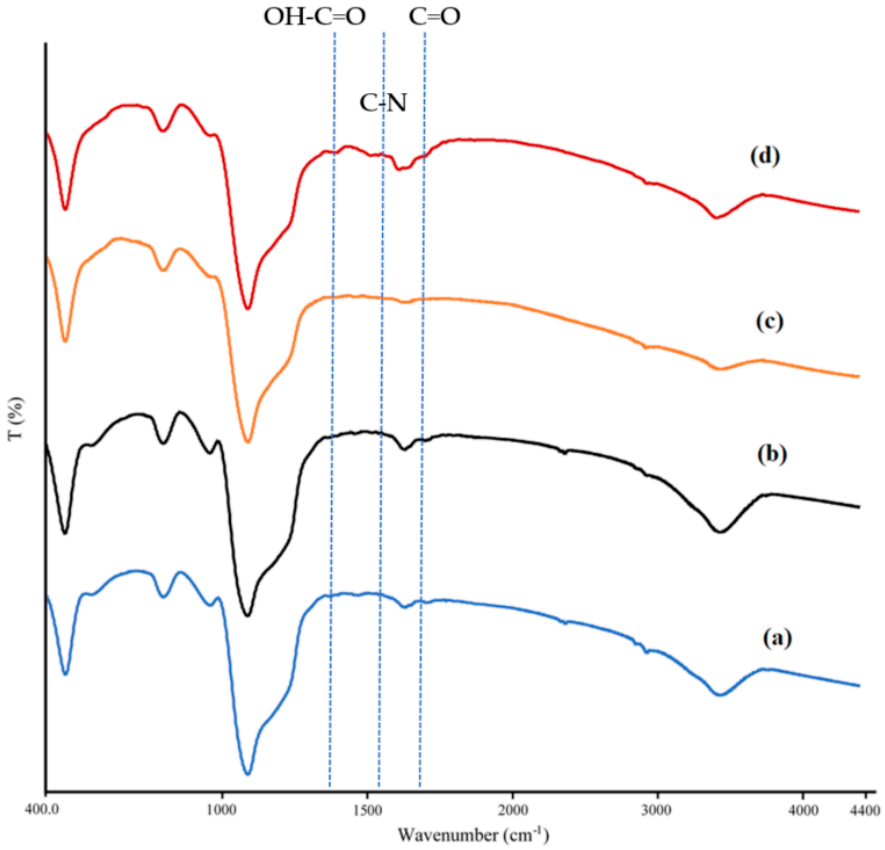

Figure 4. FT-IR spectra of: (**a**) as made DMSNs, (**b**) DMSNs, (**c**) AP-DMSN, and (**d**) FA-DMSN.

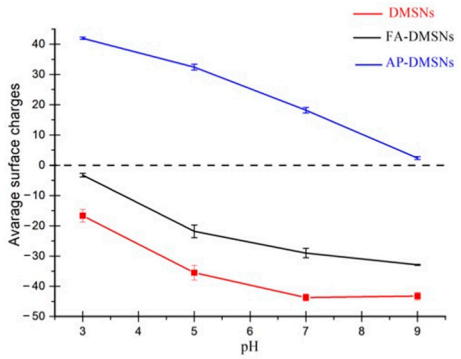

Figure 5. Zeta potential values (in mV) for AP-DMSN and FA-DMSN at different pH levels.

The thermal degradation properties of the synthesized materials were also examined using thermogravimetric analysis. As shown in Figure 6, a large mass loss of 23% was observed for the as made DMSNs, and approximately 4%, 6%, and 19% of mass losses were obtained for DMSNs, AP-DMSNs, and FA-DMSNs, respectively. The first loss of mass, which occurred below 225 °C, could be attributed to the evaporation of the adsorbed residual solvent molecules and water moisture from the DMSNs surface. The second mass loss of 15% occurred between 230 and 400 °C could be assigned to the thermal degradation of immobilized surfactant molecules. Two steps of thermal degradation of both AP-DMSNs and FA-DMSNs were consequences of the surface desorption of the amino and folic acid functional groups, respectively. This significant difference in the TGA mass loss between AP-DMSNs and FA-DMSNs indicates the successful modification of DMSNs with the folic acid functional group.

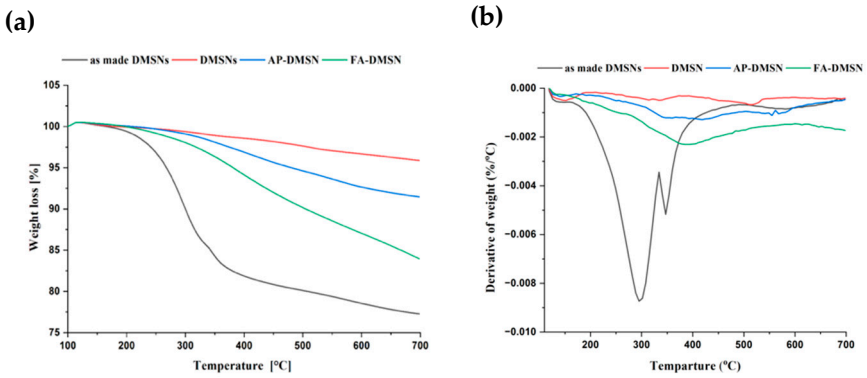

Figure 6. Thermogravimetric analysis (**a**) and derivative weight loss curves of the fabricated DMSNs (**b**).

3.2. Adsorption Studies

3.2.1. The Effect of pH on MB Removal

The pH level of water is one of the most important environmental factors that limit the applicability of most water remediation techniques. Therefore, the effect of pH on the extraction efficiency of FA-DMSN and bare DMSN was examined using pH values ranging from 3 to 9, Figure 7. The obtained experimental results show that MB largely relied on the pH, which significantly impacted both the dye's chemistry and the ionization state of the sorbent's organic functional group. The DMSNs show maximum adsorption efficiency of 30% at a high pH value, which was attributed to the electrostatic interactions between the deprotonated silanol group and the positively charged MB. In contrast, FA-DMSNs exhibited more than 95% extraction efficiency at pH > 7 and a minimum extraction efficiency of 45% at pH 3. This superb removal ability could be attributed to the synergistic effect of both the deprotonated carboxylic acid moieties and the hydrophobic sites of the folic acid backbone [45–47].

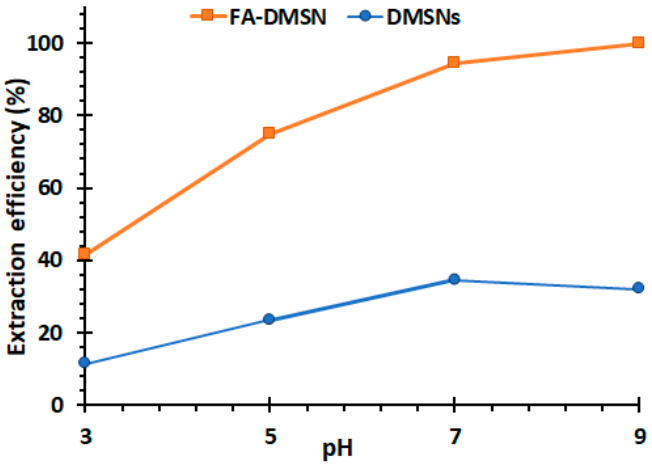

Figure 7. Influence of pH on the sorption of methylene blue (MB) dye by DMSNs and FA-DMSN at equilibrium (after normalizing).

3.2.2. Equilibrium Isotherms

The linear form of Langmuir and Freundlich isotherms for removing MP using FA-DMSNs is shown in Figure 8. According to the correlation coefficient (R^2) of both models, the obtained experimental data were fitted well with the Langmuir isotherm, indicating a monolayer adsorbate molecules surface coverage and homogeneous distribution of the adsorption sites, Figure 8b. A maximum adsorption capacity of 90.6 mg/g was determined using the Langmuir isotherm model for FA-DMSNs with an R_L value between 0 and 1, indicating a better adsorption affinity of MB ions into FA-DMSNs.

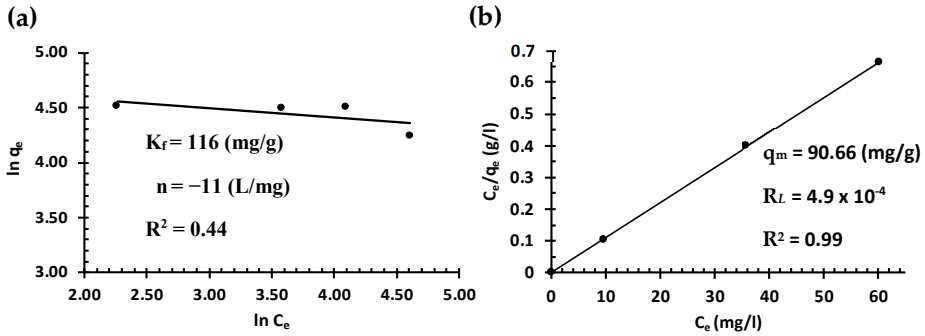

Figure 8. Methylene blue (MB) sorption at 25 °C by the fabricated FA-DMSN at equilibrium with different initial analytes concentrations. Graphs (**a**,**b**) demonstrate Freundlich and Langmuir isotherms, respectively.

A comparative evaluation of the adsorption capacity and the equilibrium time of FA-DMSNs and other sorbents for the removal of MB are listed in Table 2. The primary goals of the development of any adsorbent are the adsorption capacity and the equilibrium time. The equilibrium time for the removal of MB using FA-DMSN was reached in less than 3 min with a relatively high adsorption capacity of 90.66 mg·g^{-1}, suggesting the high potential of FA-DMSNs for the removal of organic dyes from aqueous systems compared to other materials.

Table 2. The maximum adsorption capacities (Qm) for MB sorption onto different types of adsorbents.

Sorbent	Equilibrium Time	Q_m (mg/g)	Ref.
Monodispersed MSNs	within 6 min	38.17	[45]
MIL-53(Al)-NH_2	300 min	188.60	[46]
Fe_3O_4@MIL-53(Al)	180 min	148.80	[47]
Green olive stones	24 h	588.20	[48]
Black olive stones	24 h	476.20	
CMMSNs	300 min	120.0	[49]
MCM-41	60 min	65.70	[50]
CuO/MCM-41	60 min	87.80	
FA-DMSN	within 3 min	90.66	This work

3.2.3. Effect of Adsorption Time and Adsorption Kinetics

A kinetic study was conducted to see how the analyte would interact with these unique morphological characteristics of DMSNs compared to conventional silica nanoparticles; 10 mg of FA-DMSNs was added to different solutions of MB with a concentration ranging from 50 to 125 ug.cm^{-3}. Kinetic models, such as pseudo-first-order and pseudo-second-order models have been applied to the experimental data, and their applicability and consistency depend upon the calculated correlation coefficients. As shown in Figure 9A,B, the sorption data does not fit well with the pseudo-first-order model but best fits the pseudo-second-order kinetic equation with a correlation coefficient of more than 0.99. This indicates that the rate-limiting step in the adsorption mechanism is a chemisorption process. In this mechanism, the diffusion process depends on the adsorbent capacity and not on the adsorbate dose [51]. In addition to these models, the intraparticle diffusion model has also been used to describe the diffusion-controlled adsorption kinetics, Figure 9C. Two distinct kinetic steps were obtained, showing that both film and intraparticle diffusion control the adsorption of MB ions into the FA-DMSNs. The fast intra-particle diffusion could be attributed to the large pore size of DMSNs, in which the diffusion of the analytes into the pores relies upon their size and structure [52,53].

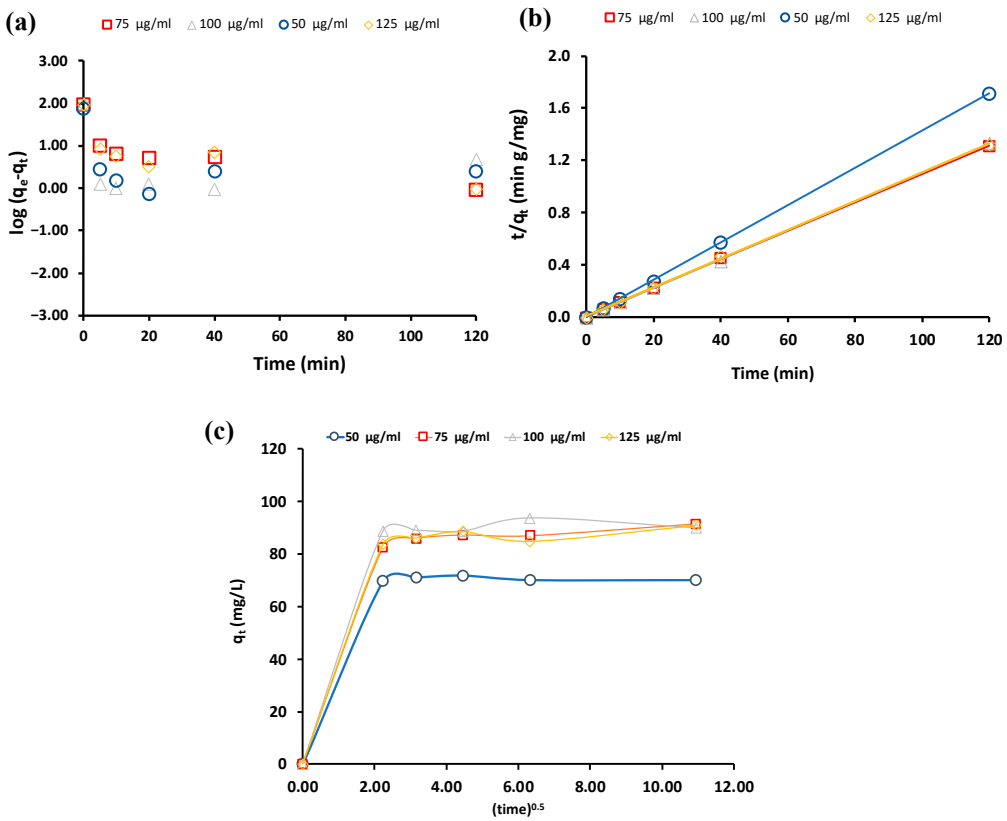

Figure 9. (**a**,**b**) Pseudo-first-order and pseudo-second-order models of methylene blue (MB) sorption by FA-DMSN, respectively; (**c**) intraparticle diffusion model of MB by FA-DMSN.

4. Conclusions

In this study, dendritic mesoporous silica nanoparticles were synthesized and modified with a folic acid functional group for the removal of methylene blue (MB) from aqueous solutions. The synthesized DMSNs exhibit a high surface area (521 m^2 g^{-1}) and pore volume (1.2 cm^3 g^{-1}). It features both wide pore size and narrow distributions, which strongly affect the adsorption performance in terms of the equilibrium uptake time. The extraction efficiency of the modified DMSNs (FA-DMSN) was found to be three times more effective than the bare DMSN materials, with a maximum adsorption capacity of 90.7 mg/g. The intra−particle diffusion model revealed a significantly fast intra-particle diffusion which can be attributed to the presence of the large pore's channels.

Author Contributions: Methodology; validation; formal analysis; investigation; data curation; writing—original draft preparation; writing—review and editing; supervision; project administration A.A.A., K.M.A. and A.M.A.; formal analysis H.S.A.; funding acquisition, A.M.A. All authors have read and agreed to the published version of the manuscript.

Funding: This research received no external funding.

Informed Consent Statement: Not applicable.

Data Availability Statement: Not applicable.

Acknowledgments: The authors thank Researchers Supporting Project number (RSP-2021/242), King Saud University, Riyadh, Saudi Arabia.

Conflicts of Interest: The authors declare no conflict of interest.

References

1. Bhatia, S.C. *Pollution Control in Textile Industry*, 1st ed.; Devraj, S., Ed.; Woodhead Publishing India Pvt. Ltd.: New Delhi, India, 2017; Volume 4, ISBN 978-1-351-37306-7.
2. Hassan, M.M.; Carr, C.M. A Critical Review on Recent Advancements of the Removal of Reactive Dyes from Dyehouse Effluent by Ion-Exchange Adsorbents. *Chemosphere* **2018**, *209*, 201–219. [CrossRef] [PubMed]
3. Imran, M.; Crowley, D.E.; Khalid, A.; Hussain, S.; Mumtaz, M.W.; Arshad, M. Microbial Biotechnology for Decolorization of Textile Wastewaters. *Rev. Environ. Sci. Biotechnol.* **2015**, *14*, 73–92. [CrossRef]
4. Nippatla, N.; Philip, L. Electrocoagulation-Floatation Assisted Pulsed Power Plasma Technology for the Complete Mineralization of Potentially Toxic Dyes and Real Textile Wastewater. *Process. Saf. Environ. Prot.* **2019**, *125*, 143–156. [CrossRef]
5. Meerbergen, K.; Crauwels, S.; Willems, K.A.; Dewil, R.; Van Impe, J.; Appels, L.; Lievens, B. Decolorization of Reactive Azo Dyes Using a Sequential Chemical and Activated Sludge Treatment. *J. Biosci. Bioeng.* **2017**, *124*, 668–673. [CrossRef] [PubMed]
6. Dong, B.; Chen, H.; Yang, Y.; He, Q.; Dai, X. Treatment of Printing and Dyeing Wastewater Using MBBR Followed by Membrane Separation Process. *Desalin. Water Treat.* **2014**, *52*, 4562–4567. [CrossRef]
7. Rachna, K.; Agarwal, A.; Singh, N. Rice Husk and Sodium Hydroxide Activated Rice Husk for Removal of Reactive Yellow Dye from Water. *Mater. Today Proc.* **2019**, *12*, 573–580. [CrossRef]
8. Alotaibi, K.M. Mesoporous Silica Nanoparticles Modified with Stimuli-Responsive Polymer Brush as an Efficient Adsorbent for Chlorophenoxy Herbicides Removal from Contaminated Water. *Int. J. Environ. Anal. Chem.* **2021**, 1–14. [CrossRef]
9. Alotaibi, A.A.; Shukla, A.K.; Mrad, M.H.; Alswieleh, A.M.; Alotaibi, K.M. Fabrication of Polysulfone-Surface Functionalized Mesoporous Silica Nanocomposite Membranes for Removal of Heavy Metal Ions from Wastewater. *Membranes* **2021**, *11*, 935. [CrossRef] [PubMed]
10. Beagan, A.; Alotaibi, K.; Almakhlafi, M.; Algarabli, W.; Alajmi, N.; Alanazi, M.; Alwaalah, H.; Alharbi, F.; Alshammari, R.; Alswieleh, A. Amine and Sulfonic Acid Functionalized Mesoporous Silica as an Effective Adsorbent for Removal of Methylene Blue from Contaminated Water. *J. King Saud Univ. Sci.* **2022**, *34*, 101762. [CrossRef]
11. Standeker, S.; Novak, Z.; Knez, Z. Adsorption of Toxic Organic Compounds from Water with Hydrophobic Silica Aerogels. *J. Colloid Interface Sci.* **2007**, *310*, 362–368. [CrossRef] [PubMed]
12. Caputo, G.; De Marco, I.; Reverchon, E. Silica Aerogel–Metal Composites Produced by Supercritical Adsorption. *J. Supercrit. Fluids* **2010**, *54*, 243–249. [CrossRef]
13. Alotaibi, K.M.; Shiels, L.; Lacaze, L.; Peshkur, T.A.; Anderson, P.; Machala, L.; Critchley, K.; Patwardhan, S.V.; Gibson, L.T. Iron Supported on Bioinspired Green Silica for Water Remediation. *Chem. Sci.* **2016**, *8*, 567–576. [CrossRef] [PubMed]
14. Idris, S.A.; Alotaibi, K.; Peshkur, T.A.; Anderson, P.; Gibson, L.T. Preconcentration and Selective Extraction of Chromium Species in Water Samples Using Amino Modified Mesoporous Silica. *J. Colloid Interface Sci.* **2012**, *386*, 344–349. [CrossRef] [PubMed]
15. Polshettiwar, V.; Cha, D.; Zhang, X.; Basset, J.M. High-Surface-Area Silica Nanospheres (KCC-1) with a Fibrous Morphology. *Angew. Chemie* **2010**, *122*, 9846–9850. [CrossRef]
16. Polshettiwar, V.; Basset, J.-M. High Surface Area Fibrous Silica Nanoparticles. U.S. Patant US 8,883,308 B2, 11 November 2014.
17. Kienzle, A.; Kurch, S.; Schlöder, J.; Berges, C.; Ose, R.; Schupp, J.; Tuettenberg, A.; Weiss, H.; Schultze, J.; Winzen, S.; et al. Dendritic Mesoporous Silica Nanoparticles for PH-Stimuli-Responsive Drug Delivery of TNF-Alpha. *Adv. Healthc. Mater.* **2017**, *6*, 1700012. [CrossRef] [PubMed]
18. Vallet-Regí, M.; Izquierdo-Barba, I.; Colilla, M. Structure and Functionalization of Mesoporous Bioceramics for Bone Tissue Regeneration and Local Drug Delivery. *Philos. Trans. R. Soc. A Math. Phys. Eng. Sci.* **2012**, *370*, 1400–1421. [CrossRef] [PubMed]
19. Argyo, C.; Weiss, V.; Bräuchle, C.; Bein, T. Multifunctional Mesoporous Silica Nanoparticles as a Universal Platform for Drug Delivery. *Chem. Mater.* **2014**, *26*, 435–451. [CrossRef]
20. Mahmudi, M.; Shadjou, N.; Hasanzadeh, M. Synthesis and Adsorption Behavior of Dendritic Fibrous Nano-Silica (DFNS) Grafted by d-Penicillamine as an Advanced Nanomaterial for the Removal of Some Metal Ions from Contaminated Water. *J. Electroanal. Chem.* **2019**, *848*, 113272. [CrossRef]
21. Nia, M.H.; Kiasat, A.R.; van de Ven, T.G.M. Dendritic Fibrous Colloidal Silica Internally Cross-Linked by Bivalent Organic Cations: An Efficient Support for Dye Removal and the Reduction of Nitrobenzene Derivatives. *Langmuir* **2021**, *37*, 13676–13688. [CrossRef] [PubMed]
22. Abbasvash, L.; Shadjou, N. Synthesize of β-Cyclodextrin Functionalized Dendritic Fibrous Nanosilica and Its Application for the Removal of Organic Dye (Malachite Green). *J. Mol. Recognit.* **2020**, *33*, e2850. [CrossRef] [PubMed]
23. Stewart, C.F.; Zamboni, W.C.; Crom, W.R.; Gajjar, A.; Heideman, R.L.; Furman, W.L.; Meyer, W.H.; Houghton, P.J.; Pratt, C.B. Topoisomerase I Interactive Drugs in Children with Cancer. *Invest. New Drugs* **1996**, *14*, 37–47. [CrossRef] [PubMed]
24. AbouAitah, K.; Swiderska-Sroda, A.; Farghali, A.A.; Wojnarowicz, J.; Stefanek, A.; Gierlotka, S.; Opalinska, A.; Allayeh, A.K.; Ciach, T.; Lojkowski, W. Folic Acid-Conjugated Mesoporous Silica Particles as Nanocarriers of Natural Prodrugs for Cancer Targeting and Antioxidant Action. *Oncotarget* **2018**, *9*, 26466–26490. [CrossRef] [PubMed]
25. Qu, W.; Meng, B.; Yu, Y.; Wang, S. Folic Acid-Conjugated Mesoporous Silica Nanoparticles for Enhanced Therapeutic Efficacy of Topotecan in Retina Cancers. *Int. J. Nanomed.* **2018**, *13*, 4379–4389. [CrossRef] [PubMed]
26. Li, X.; Chen, X.; Miao, G.; Liu, H.; Mao, C.; Yuan, G.; Liang, Q.; Shen, X.; Ning, C.; Fu, X. Synthesis of Radial Mesoporous Bioactive Glass Particles to Deliver Osteoactivin Gene. *J. Mater. Chem. B* **2014**, *2*, 7045–7054. [CrossRef]

27. Beagan, A.M.; Alghamdi, A.A.; Lahmadi, S.S.; Halwani, M.A.; Almeataq, M.S.; Alhazaa, A.N.; Alotaibi, K.M.; Alswieleh, A.M. Folic Acid-Terminated Poly(2-Diethyl Amino Ethyl Methacrylate) Brush-Gated Magnetic Mesoporous Nanoparticles as a Smart Drug Delivery System. *Polymers* **2021**, *13*, 59. [CrossRef]
28. Ji, J.; Wu, D.; Liu, L.; Chen, J.; Xu, Y. Preparation, Characterization, and in Vitro Release of Folic Acid-Conjugated Chitosan Nanoparticles Loaded with Methotrexate for Targeted Delivery. *Polym. Bull.* **2012**, *68*, 1707–1720. [CrossRef]
29. Alotaibi, K.M.; Almethen, A.A.; Beagan, A.M.; Al-Swaidan, H.M.; Ahmad, A.; Bhawani, S.A.; Alswieleh, A.M. Quaternization of Poly (2-Diethyl Aminoethyl Methacrylate) Brush-Grafted Magnetic Mesoporous Nanoparticles Using 2-Iodoethanol for Removing Anionic Dyes. *Appl. Sci.* **2021**, *11*, 10451. [CrossRef]
30. Abdeen, Z.; Mohammad, S.G. Study of the Adsorption Efficiency of an Eco-Friendly Carbohydrate Polymer for Contaminated Aqueous Solution by Organophosphorus Pesticide. *Open J. Org. Polym. Mater.* **2014**, *4*, 16–28. [CrossRef]
31. Kiurski, J.; Adamovic, S.; Krstic, J.; Oros, I.; Vojinovic Miloradov, M. Adsorption Efficiency of Low-Cost Materials in the Removal of Zn (II) Ions from Printing Developer. *Acta Tech. Corviniensis Bull. Eng.* **2011**, *4*, 61–66.
32. Alaqarbeh, M. Adsorption Phenomena: Definition, Mechanisms, and Adsorption Types: Short Review. *RHAZES Green Appl. Chem.* **2021**, *13*, 43–51.
33. Ho, Y.S.; McKay, G. Application of Kinetic Models to the Sorption of Copper(II) on to Peat. *Adsorpt. Sci. Technol.* **2002**, *20*, 797–815. [CrossRef]
34. I IARC Working Group on the Evaluation of Carcinogenic Risks to Humans. *Arsenic, Metals, Fibres and Dusts*; International Agency for Research on Cancer: Lyon, France, 2012; Volume 100, ISBN 978 92 832 1320 8.
35. Ho, Y.-S. Second-Order Kinetic Model for the Sorption of Cadmium onto Tree Fern: A Comparison of Linear and Non-Linear Methods. *Water Res.* **2006**, *40*, 119–125. [CrossRef] [PubMed]
36. Weber, W.J.; Morris, J.C. Kinetics of Adsorption on Carbon from Solution. *J. Sanit. Eng. Div.* **1963**, *89*, 31–59. [CrossRef]
37. Sen Gupta, S.; Bhattacharyya, K.G. Kinetics of Adsorption of Metal Ions on Inorganic Materials: A Review. *Adv. Colloid Interface Sci.* **2011**, *162*, 39–58. [CrossRef] [PubMed]
38. Febrianto, J.; Kosasih, A.N.; Sunarso, J.; Ju, Y.H.; Indraswati, N.; Ismadji, S. Equilibrium and Kinetic Studies in Adsorption of Heavy Metals Using Biosorbent: A Summary of Recent Studies. *J. Hazard. Mater.* **2009**, *162*, 616–645. [CrossRef] [PubMed]
39. Thommes, M.; Kaneko, K.; Neimark, A.V.; Olivier, J.P.; Rodriguez-Reinoso, F.; Rouquerol, J.; Sing, K.S.W. Physisorption of Gases, with Special Reference to the Evaluation of Surface Area and Pore Size Distribution (IUPAC Technical Report). *Pure Appl. Chem.* **2015**, *87*, 1051–1069. [CrossRef]
40. Shen, D.; Yang, J.; Li, X.; Zhou, L.; Zhang, R.; Li, W.; Chen, L.; Wang, R.; Zhang, F.; Zhao, D. Biphase Stratification Approach to Three-Dimensional Dendritic Biodegradable Mesoporous Silica Nanospheres. *Nano Lett.* **2014**, *14*, 923–932. [CrossRef]
41. Alswieleh, A.M.; Beagan, A.M.; Alsheheri, B.M.; Alotaibi, K.M.; Alharthi, M.D.; Almeataq, M.S. Hybrid Mesoporous Silica Nanoparticles Grafted with 2-(Tert-Butylamino)Ethyl Methacrylate-b-Poly(Ethylene Glycol) Methyl Ether Methacrylate Diblock Brushes as Drug Nanocarrier. *Molecules* **2020**, *25*, 195. [CrossRef]
42. Beagan, A.M. Investigating Methylene Blue Removal from Aqueous Solution by Cysteine-Functionalized Mesoporous Silica. *J. Chem.* **2021**, *2021*, 8839864. [CrossRef]
43. Trukawka, M.; Cendrowski, K.; Konicki, W.; Mijowska, E. Folic Acid/Methotrexate Functionalized Mesoporous Silica Nanoflakes from Different Supports: Comparative Study. *Appl. Sci.* **2020**, *10*, 6465. [CrossRef]
44. Bandara, S.; Carnegie, C.-a.; Johnson, C.; Akindoju, F.; Williams, E.; Swaby, J.M.; Oki, A.; Carson, L.E. Synthesis and Characterization of Zinc/Chitosan-Folic Acid Complex. *Heliyon* **2018**, *4*, e00737. [CrossRef]
45. Qin, P.; Yang, Y.; Zhang, X.; Niu, J.; Yang, H.; Tian, S.; Zhu, J.; Lu, M. Highly Efficient, Rapid, and Simultaneous Removal of Cationic Dyes from Aqueous Solution Using Monodispersed Mesoporous Silica Nanoparticles as the Adsorbent. *Nanomaterials* **2018**, *8*, 4. [CrossRef] [PubMed]
46. Li, C.; Xiong, Z.; Zhang, J.; Wu, C. The Strengthening Role of the Amino Group in Metal–Organic Framework MIL-53 (Al) for Methylene Blue and Malachite Green Dye Adsorption. *J. Chem. Eng. Data* **2015**, *60*, 3414–3422. [CrossRef]
47. Zhang, G.; Wo, R.; Sun, Z.; Hao, G.; Liu, G.; Zhang, Y.; Guo, H.; Jiang, W. Effective Magnetic Mofs Adsorbent for the Removal of Bisphenol a, Tetracycline, Congo Red and Methylene Blue Pollutions. *Nanomaterials* **2021**, *11*, 1917. [CrossRef] [PubMed]
48. Al-Ghouti, M.A.; Al-Absi, R.S. Mechanistic Understanding of the Adsorption and Thermodynamic Aspects of Cationic Methylene Blue Dye onto Cellulosic Olive Stones Biomass from Wastewater. *Sci. Rep.* **2020**, *10*, 15928. [CrossRef] [PubMed]
49. Li, Y.; Zhou, Y.; Nie, W.; Song, L.; Chen, P. Highly Efficient Methylene Blue Dyes Removal from Aqueous Systems by Chitosan Coated Magnetic Mesoporous Silica Nanoparticles. *J. Porous Mater.* **2015**, *22*, 1383–1392. [CrossRef]
50. Liang, Z.; Zhao, Z.; Sun, T.; Shi, W.; Cui, F. Enhanced Adsorption of the Cationic Dyes in the Spherical CuO/Meso-Silica Nano Composite and Impact of Solution Chemistry. *J. Colloid Interface Sci.* **2017**, *485*, 192–200. [CrossRef] [PubMed]
51. Sahoo, T.R.; Prelot, B. Adsorption Processes for the Removal of Contaminants from Wastewater: The Perspective Role of Nanomaterials and Nanotechnology. In *Micro and Nano Technologies*; Bonelli, B., Freyria, F.S., Rossetti, I., Sethi, R.B.T.-N., Eds.; Chapter 7; Elsevier: Amsterdam, The Netherlands, 2020; pp. 161–222. ISBN 978-0-12-818489-9.
52. Lee, S.Y.; Seader, J.D.; Tsai, C.H.; Massoth, F.E. Restrictive Liquid-Phase Diffusion and Reaction in Bidisperse Catalysts. *Ind. Eng. Chem. Res.* **1991**, *30*, 1683–1693. [CrossRef]
53. PAPPENHEIMER, J.R. Passage of Molecules through Capillary Wals. *Physiol. Rev.* **1953**, *33*, 387–423. [CrossRef] [PubMed]